

## P5.1 GENERATION OF FREE CONVECTION IN A VALLEY DUE TO CHANGES OF THE LOCAL CIRCULATION SYSTEM

Rafael Eigenmann\*, Stefan Metzger, Lukas Siebicke, Katharina Staudt, Andrei Serafimovich, Thomas Foken

University of Bayreuth, BayCEER, Department of Micrometeorology, Bayreuth, Germany

### 1. INTRODUCTION

Surface energy exchange measurements of two energy balance stations installed from June 1 to August 31, 2007 during the COPS (Convective and Orographically-induced Precipitation Study) field campaign in the Kinzig valley within the low mountain range of the Black Forest are used to investigate the generation of free convection events (FCEs) initiated by a change of the local circulation system. These FCEs are assumed to have an essential impact on ABL thermodynamics and structure. Recently, Mayer et al. (2008) observed FCEs, which originated from a valley and led to a strong and sudden ozone decrease at a mountain summit (Hohenpeissenberg) in the morning hours. In their study, the FCEs were found to be triggered by a simultaneously occurring wind speed minimum facilitating the conditions for free convection. On about half of the days these wind speed minima could be attributed to the onset of Alpine Pumping in the alpine foreland (Winkler et al., 2006; Lugauer and Winkler, 2005) associated with a change of wind direction causing a drop of the horizontal wind speed. Hence, other meso-scale or local circulation systems initiated by complex terrain are expected to trigger FCEs. In the Kinzig valley, a clear diurnal thermally-induced valley wind system was observed (e.g. Meißner et al., 2007), thus providing the opportunity to check whether or not such vigorous vertical transport mechanisms are sufficiently captured by common flux measurement techniques (Mayer et al., 2008), e.g. the eddy-covariance (EC) method.

To sum up, this study demonstrates the profound quality assurance and control effort adapted to the energy exchange measurements and its applicability to the selection and description of free convection events (FCEs).

\*Corresponding author address:

Rafael Eigenmann, University of Bayreuth, Department of Micrometeorology, 95440 Bayreuth, Germany; e-mail: [rafael.eigenmann@uni-bayreuth.de](mailto:rafael.eigenmann@uni-bayreuth.de)

### 2. COPS ENERGY BALANCE NETWORK

The COPS project initiated within the German 6-year Priority Program 1167 'Quantitative Precipitation Forecast PQP (Praecipitationis Quantitativae Predictio)' funded by the German Science Foundation (DFG) aims to identify the physical and chemical processes responsible for the deficiencies in QPF (Quantitative Precipitation Forecast) over low-mountain regions and to advance the quality of forecasts of orographically-induced convective precipitation by 4D observations and modeling of its life cycle (Wulfmeyer et al., 2007). Within COPS, the University of Bayreuth coordinates the energy balance network aiming at providing surface flux and other surface quantity data of the required high accuracy and quality for the scientific community in general, but particularly for the forcing and validation of applied meso-scale models within COPS. Figure 1 shows all collaborating institutes within the energy balance network with both of the stations under investigation in the Kinzig valley, i.e. BT01ETGS (Fußbach) and BT04ETG (Hagenbuch), highlighted.

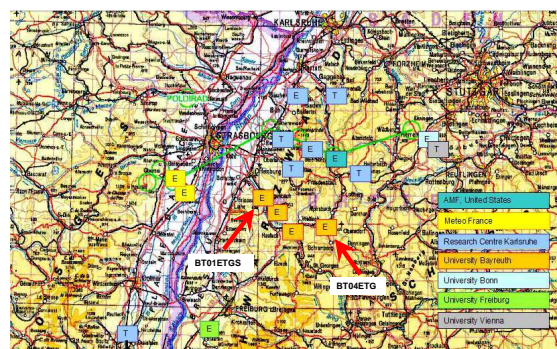


Figure 1: Topographic map of the COPS region with the measurement locations of the participating institutes of the energy balance network (<http://www.bayceer.uni-bayreuth.de/COPS/>). The four energy balance stations of the University of Bayreuth are installed in the Kinzig valley with both of the sites investigated in this study, i.e. BT01ETGS (Fußbach) and BT04ETG (Hagenbuch), indicated by red arrows.

### 3. EXPERIMENT SETUP

Both energy balance stations in the Kinzig valley, i.e. BT01ETGS (48°22'7.8"N, 8°1'21.2"E, 178 m a.s.l.) and BT04ETG (48°16'54.6"N, 8°12'16.8"E, 245 m a.s.l.) measured, above a corn field and a meadow respectively, high-frequency (20 Hz) turbulent fluxes for momentum, sensible and latent heat as well as CO<sub>2</sub> using a CSAT3 (Campbell Scientific, Inc.) sonic anemometer for recording wind vector and sonic temperature T<sub>s</sub> and a LI-7500 (LI-COR Biosciences) open-path gas analyser for water vapor H<sub>2</sub>O and carbon dioxide CO<sub>2</sub> concentrations. The measurement height at BT01ETGS was adjusted to the growing corn field, whereas at BT04ETG it had a constant value of 2.5 m a.g.l. Short-wave components of the net radiation were measured with a CM24 (Kipp&Zonen) at BT01ETGS, long-wave components with an Eppley PIR (Eppley Laboratory, Inc.). Both sensors are adjusted to canopy heights. At BT04ETG a CNR1 (Kipp&Zonen) net radiometer is used at a constant height of 1.92 m a.g.l. Both sites record the soil heat flux at 0.1 m depth with a HFP01SC (Hukseflux Thermal Sensors) heat flux plate, the soil temperature at 0.02, 0.05, 0.1 and 0.2 m depth with PT100 soil thermometers and the soil moisture at 0.05 and 0.2 m depth with a TRIME (IMKO GmbH) TDR probe. Additionally, the ABL structure was detected at BT01ETGS by acoustic and radioacoustic sounding measurements applying a phase array Doppler Sodar DSDPA.90-64 with a 1290-MHz- RASS extension by Metek GmbH. Furthermore, a pressure sensor P6520 (Ammonit) and a 9 m profile mast equipped at six different heights with F460 cup anemometers (Climatronics) and Frankenberger psychrometers were installed at BT01ETGS. Detailed information about the measuring set up and background data can be obtained from the COPS experiment documentation of the University of Bayreuth (Metzger et al., 2007).

### 4. ENERGY EXCHANGE MEASUREMENTS

The energy flux data measured at BT01ETGS and BT04ETG were processed and quality controlled applying latest micrometeorological post-field data processing protocols (e.g. Mauder et al., 2006) in order to obtain a data set of the desired quality and accuracy, which can be utilized for further fundamental research. Accordingly, the turbulent flux raw data recorded with the eddy-covariance (EC) method were post-processed with

the comprehensive software package TK2 developed at the University of Bayreuth (Mauder and Foken, 2004), which comprises all state of the art flux corrections and post-field quality control including tests for steady state and developed turbulence (Foken and Wichura, 1996; Foken et al., 2004). Theoretical assumptions actually restrict the EC method to homogeneous terrain, but the increasing demand of continuous monitoring of flux data (Aubinet et al., 2000; Baldocchi et al., 2001) forced the application of the EC method within highly structured terrain also assignable to the COPS region. This step is supported by the development of a valuable site evaluation and characterisation approach (Göckede et al., 2004, 2006), which combines the flux data quality approach (Foken et al., 2004) with a forward Lagrangian footprint model (Rannik et al., 2000, 2003), able to identify site-specific spatial quality structures and the spatial representivity of the measured flux data in the context of the underlying land use distribution. This approach has been recently employed on sites of the CarboEurope-IP network by Rebmann et al. (2005) and Göckede et al. (2008) and is used in this study – together with a check for possible internal boundary layers – in order to obtain target land use type-representative turbulent flux data sets of the required high quality usable by the COPS community for further analysis.

In the following, only the results of BT01ETGS are presented. The evaluation of BT04ETG led to similar findings (Eigenmann, 2008).

Figure 2 depicts the processed turbulent fluxes of sensible (Q<sub>H</sub>) and latent heat (Q<sub>E</sub>), friction velocity  $u_*$  as well as the CO<sub>2</sub> net ecosystem exchange (NEE) in a diurnal vs. annual resolution over the entire measurement period at BT01ETGS, where the attached color bar represents the calculated values. The footprint climatology as related to land use distribution at BT01ETGS is visualized in Figure 3 and reveals good spatial representivity of the flux measurements, as the 5 % effect level ring lies within the corn field regardless of stratification. A relatively small footprint was found at BT01ETGS, which can be ascribed to the fast growing corn field resulting in low effective measurement heights and high roughness length, thus reducing its extension. The footprint climatology is slightly elongated in the main wind direction in the north-south oriented Kinzig valley at BT01ETGS. The spatial distribution of quality flags as related to footprint climatology depending on stability is depicted in Figure 4 for the case of momentum

flux. Within the 5% effect level ring, quality ratings mainly consist of class 1 and 2 being suitable for fundamental research. However, towards the valley sidewalls degraded flagging is found for all turbulent fluxes at both sites.

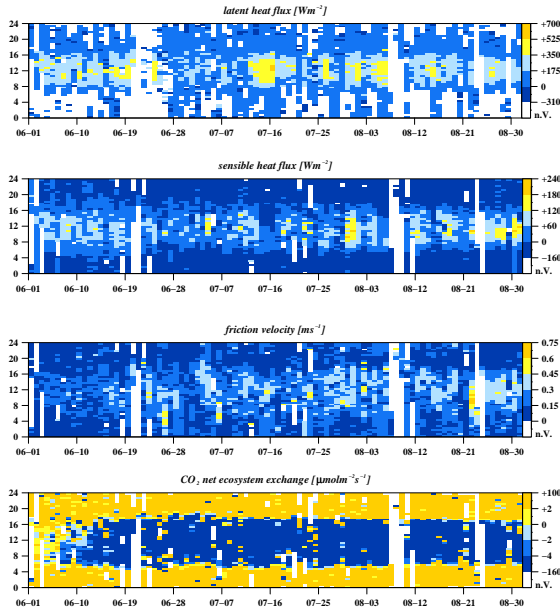


Figure 2: Sensible heat flux  $Q_H$  [ $Wm^{-2}$ ], latent heat flux  $Q_E$  [ $Wm^{-2}$ ], friction velocity  $u^*$  [ $ms^{-1}$ ] and  $CO_2$  NEE [ $\mu molm^{-2}s^{-1}$ ] for the entire measurement period at BT01ETGS: X-axis represents the day of the year, Y-axis the time of the day [UTC] and the attached color bar the calculated values.

To gain insight into the average flux contribution of the target land use type, i.e. corn at BT01ETGS, as a function of different wind sectors and stability classes, appropriate sorted data have been individually processed within the footprint analysis. The results are listed in Table 1 and reveal good average flux contributions of more than 92% for all wind sectors during unstable or neutral cases. However, for stable stratification easterly and westerly sectors have to be considered critically, as flux contributions below 80% can be found, with the minimum (67%) in the  $240^\circ$  wind sector. Admittedly, the latter finding has to be regarded with the knowledge that the density of available data is low in the easterly and westerly wind sectors as these do not lie within the main wind direction, thus weakening its influence on the overall assessment. Furthermore, a check for internal boundary layers resulting from changes of the underlying surface characteristics is also depicted in Table 1. Therefore, the following fetch-height relation was used to roughly estimate the

height of the new equilibrium layer  $\delta$  depending on fetch  $x$  (Raabe, 1983; Jegede and Foken, 1999):

$$z_a \leq \delta = 0.3\sqrt{x} \quad (1)$$

The average aerodynamic measurement height  $z_a$  of the different periods  $p$  followed by an index introduced in order to match seasonal plant growth should be lower than  $\delta$ , in order to guarantee that the measurement takes place within the new equilibrium layer established over the target land use type. Referring to Table 1, the  $270^\circ$  sector shows—for both periods  $p$ —a greater aerodynamic measurement height  $z_a$  compared to  $\delta$ , thus indicating that the flux measurements within this sector cannot be associated with the target land use type corn. Also the data of the  $240^\circ$  sector should be discarded, as  $\delta$  falls below  $z_a$  for period  $p2$  and is only slightly greater for period  $p1$ .

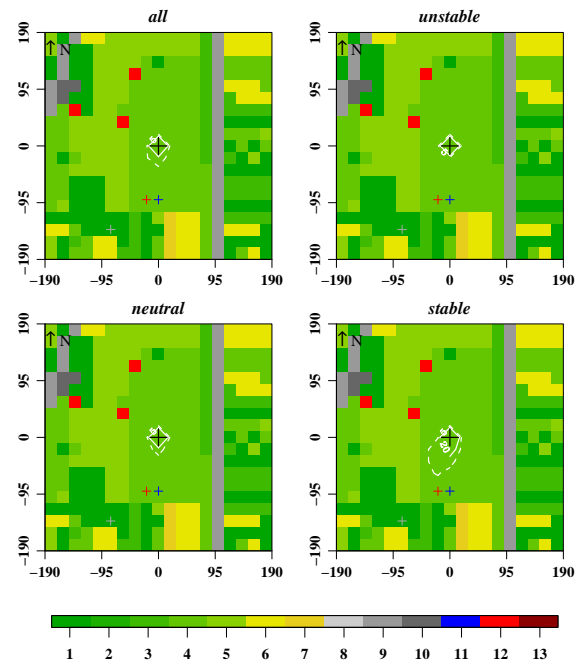


Figure 3: Land use classes as related to the footprint climatology depending on atmospheric stratification for BT01ETGS. EC tower position is indicated by the central, black crosshair, whereas the additional crosshairs indicate the position of the profile mast (blue), the radiation and soil measurement complex (red) and the Sodar/RASS system (grey). X- and Y-axis display the distance [m] from the central tower. Land use classes are distinguished according to the color bar: 1:= deciduous tree, 2:= conifer, 3:= topinambur, 4:=corn (target land use type), 5:=meadow, 6:=acre/fallow, 7:=garden, 8:=slope, 9:=street, 10:= building, 11:= stream, 12:= power pole small, 13:= power pole large. The white contour lines indicate the 5% (dashed) and 20% (solid) effect level rings of the measurements.

Table 1: Average flux contribution [%] from the target land use type corn depending on wind sector and stability class at BT01ETGS. Flux contributions for each half-hourly measurement have been calculated for periods p1 and p2 separately and then merged together for the determination of the average flux contributions denoted. Internal boundary layer heights  $\bar{\delta}$  calculated according to Equation 1 with fetch  $x$  are also depicted in dependence of the 12 wind direction classes distinguished. Wind sectors where  $\bar{\delta}$  falls below the aerodynamic measurement height  $z_a$  of the different periods introduced are flagged by 'X' and are shaded grey.

	30°	60°	90°	120°	150°	180°	210°	240°	270°	300°	330°	360°
Average flux contribution from target land use type (corn) in %												
Stable	92	77	82	86	86	89	86	67	73	69	84	89
Neutral	98	-	99	97	97	97	96	94	92	95	97	99
Unstable	99	100	100	100	100	99	99	99	99	99	99	100
Internal boundary layer evaluation												
$x$ [m]	141	83	68	84	113	102	89	59	49	66	101	162
$\bar{\delta}$ [m]	3,56	2,73	2,47	2,75	3,19	3,03	2,83	2,30	2,10	2,44	3,01	3,82
$z_a$ [m] for p1					←	2,14	→		X			
$z_a$ [m] for p2					←	2,35	→	X	X			

However, the above-mentioned evaluation must be regarded critically: the determination of  $\bar{\delta}$  is more a rough estimate than a matter of fact, as weak stability effects are neglected (Savelyev and Taylor, 2005) and the fast growing corn field, with its averaged fetch conditions, can only be roughly represented by the introduced periods. Nevertheless, the internal boundary layer evaluation in combination with the footprint analysis results reveals sectors of less reliability and data quality, which can be excluded from further data analysis.

The energy balance closure is addressed in Figure 5. Therefore, the sum of the turbulent fluxes  $Q_H$  and  $Q_E$  of each half-hourly measurement is plotted against the corresponding available energy values at the surface consisting of net radiation  $Q_S$  minus soil heat flux  $Q_G$ . The heat storage in the upper soil layer for the calculation of  $Q_G$  was considered applying the 'simple measurement' (SM) method after Liebethal and Foken (2007). As the red dashed line in Figure 5 indicates a balanced energy exchange at the surface, one can deduce an average non-closure of 20.6% at BT01ETGS. The imbalance can primarily be attributed to the landscape heterogeneity assignable to the COPS region inducing unconsidered low-frequency flux contributions and advective flux components (Foken, 2008b; Foken et al., 2006). Indeed, large eddy simulations (LES) studies revealed that turbulent organized structures (Kanda et al., 2004; Steinfeld et al., 2007) and secondary circulations (Inagaki et al., 2006) have an influence on the energy balance closure.

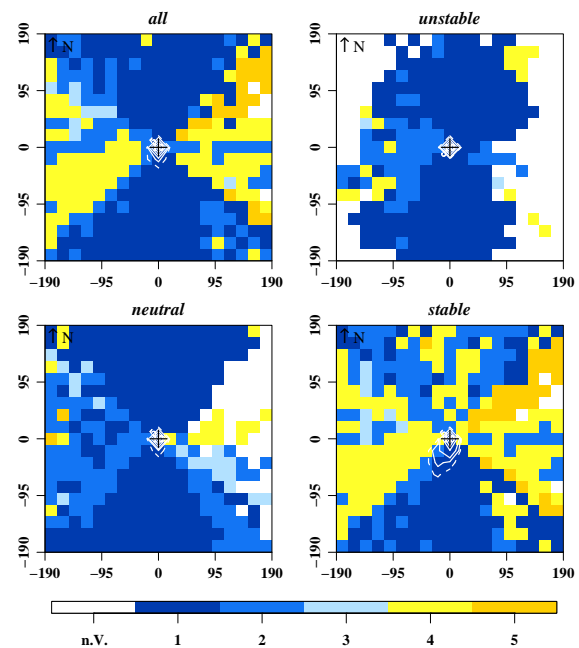


Figure 4: Spatial distribution of quality flags of the momentum flux as related to footprint climatology depending on atmospheric stratification for BT01ETGS. EC tower position is indicated by the central, black crosshair, whereas quality flags (1-5) after Rebmann et al. (2005) are distinguished according to the color bar. White contour lines display the 5% (dashed) and 10, 20, 40, 60, 80 and 100% effect level rings of the measurements.

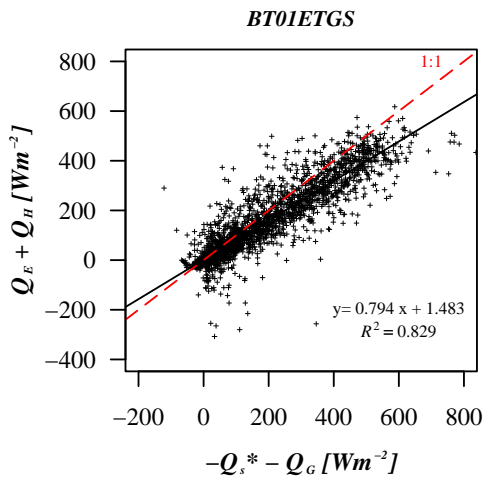


Figure 5: Relation between the available energy ( $-Q_s^* - Q_G$ ) at the surface and the sum of the both turbulent fluxes  $Q_H$  and  $Q_E$  at BT01ETGS. The regression equation and coefficient of the linear regression adapted to the scatter diagram are also denoted. The red dashed line indicates the 1:1-ratio.

## 5. GENERATION OF FREE CONVECTION

The energy exchange measurement results led to the detection of buoyantly driven free convection events (FCEs) in the morning hours at both sites under investigation (Eigenmann, 2008). Preliminary graphics produced in combination with routine data quality control during the COPS field phase consolidated recently observed indications (Mayer et al., 2008) that thermally-driven circulation systems may trigger surface-induced free convection events in the morning hours, at times the existing circulation system changes its previously prevailed wind direction. In the Kinzig valley a pronounced valley circulation system can frequently be observed to be generated in high-pressure situations with high solar radiation and weak synoptic forcing (Whiteman, 1990). At COPS IOP8b (2007-07-15) –outlined in the following as a paradigm at BT01ETGS– the Sodargramm of the wind direction in Figure 6 shows the ceasing of the down-valley, southerly winds which prevail at night and the onset of up-valley, northerly blowing winds at about 8:30 UTC near the ground. During this transition period, a strong collapse of the horizontal wind speed through the whole vertical extension of the valley atmosphere lasting from 6:30 until 8:50 UTC in the morning hours, with values smaller than  $1.5 \text{ ms}^{-1}$ , is evident from Sodar measurements (Figure 7).

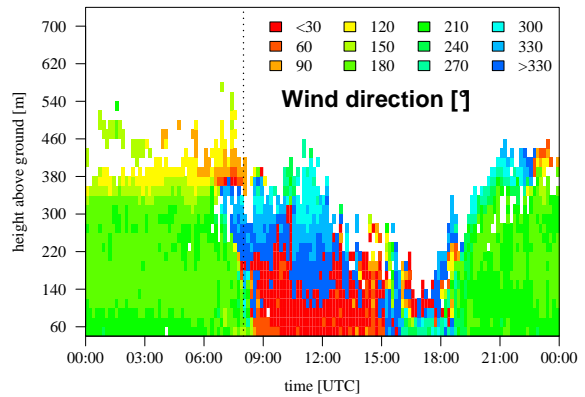


Figure 6: Sodargramm of the wind direction  $[\text{°}]$  for IOP8b at BT01ETGS. The black dotted line indicates the mean event time when  $\zeta < -1$  found in Figure 9.

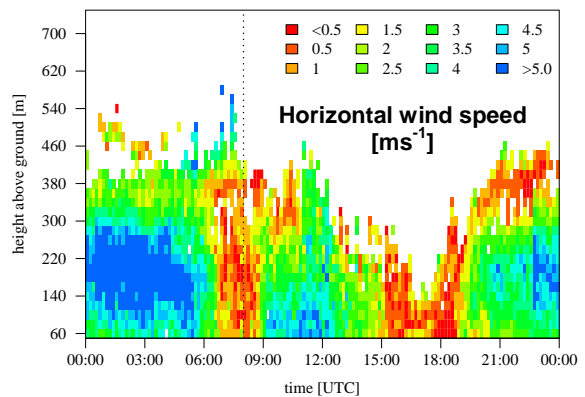


Figure 7: Sodargramm for IOP8b at BT01ETGS of the horizontal wind speed  $[\text{ms}^{-1}]$ . The black dotted line indicates the mean event time when  $\zeta < -1$  found in Figure 9.

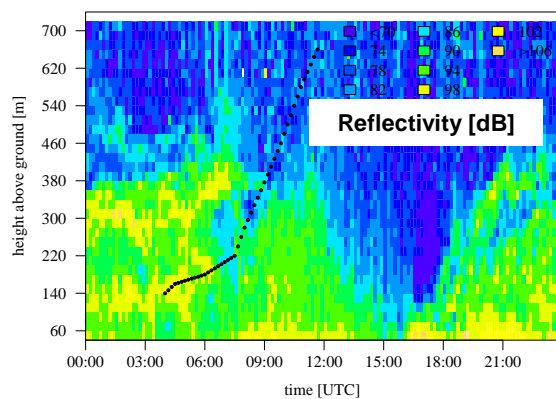


Figure 8: Sodargramm of the reflectivity  $[\text{dB}]$  and the evolution of the boundary layer depth  $z_i$  between 4:00 and 11:40 UTC (black points) for IOP8b at BT01ETGS.

The occurrence of FCEs associated with the destabilization of near-ground air masses can be detected by the EC flux measurements by calculating the stability parameter  $\zeta$  according to the following equation:

$$\zeta = \frac{z}{L} = -\frac{z \cdot \kappa \cdot g \cdot (\overline{w'\theta_v'})_0}{\overline{\theta_v} \cdot u_*^3} \quad (2)$$

where  $z$  denotes the measurement height,  $L$  the Obukhov length,  $u_*$  the friction velocity,  $g$  the acceleration due to gravity,  $\overline{\theta_v}$  the mean virtual potential temperature,  $\overline{w'\theta_v'}$  the buoyancy flux at the surface and  $\kappa$  the von-Kármán constant ( $\kappa \approx 0.4$ ). Free convection situations are indicated for  $\zeta < -1$  (Foken, 2008a) and –regarding the equation– will be facilitated for small values of  $u_*$  and high buoyancy fluxes, as buoyant forces (B) then dominate over shear forces (S) within turbulence production. Thus, the wind speed collapse in the valley (Figure 7) induced by the wind direction change (Figure 6) provides a powerful trigger mechanism for FCEs. In Figure 9a, the stability parameter  $\zeta$  is depicted, where the averaging period of the EC flux measurements and the parameters deduced from them (figure 9a-9g) was reduced from the standard 30 min to 5 min in order to gain better insight into the temporal structure of the FCEs. Events which had previously seemed to consist of one single event within the 30 min resolution interval turned out to be an accumulation of several convective pulses, of only a few minutes duration, transporting quantities of heat and moisture into the ABL. Referring to Figure 9a, a vigorous event at 7:35 - 7:40 UTC with values of  $\zeta = -9.7$  corresponds exactly with a 5 minutes duration local minima of  $u_*$  ( $0.04 \text{ ms}^{-1}$ ) in Figure 9d triggering the FCE. A second event, which can be detected from 8:10 till 8:40 UTC, shows smaller  $\zeta$  values of  $\zeta = -1.4$  but also coincides with a local minima of  $u_*$  ( $0.09 \text{ ms}^{-1}$ ). Simultaneously, high values of  $Q_H$  (Figure 9e) are found around the times of the FCEs ( $54.7 \text{ Wm}^{-2}$  at 8:25 UTC). Lower friction velocities  $u_*$  in general occur between 6:40 and 8:40 UTC explaining the generally small values of  $\zeta$  in this time, thus indicating a whole period of destabilization of ground-near air masses and their subsequent vertical transport. In addition, Figure 9i depicts the available energy at the ground ( $-Q_S - Q_G$ ) for the portioning into  $Q_H$  (Figure 9e) and  $Q_E$  (Figure 9c), which can be expressed as the Bowen ratio  $Bo$  (Figure 9f).  $Bo$  has its highest values (0.59 at 6:35 UTC) shortly before the free convection events demonstrating a preferred transformation of the available surface energy

(daily max.:  $590 \text{ Wm}^{-2}$  at 12:00 UTC) into  $Q_H$ . Other parameters such as the ratio of the Deardorff velocity  $w_*$  to  $u_*$  and the ratio of B/S have been deduced and confirm their capability to denote FCEs (Figure 9g and 9h). The Deardorff velocity  $w_*$  was calculated following Deardorff, (1970a, 1970b):

$$w_* = \left[ \frac{g \cdot z_i}{\overline{\theta_v}} (\overline{w'\theta_v'})_0 \right]^{1/3} \quad (3)$$

The depth of the boundary layer  $z_i$ , necessary to calculate  $w_*$ , is determined by visual inspection of a secondary maximum in the reflectivity profiles of the Sodar measurements (Beyrich, 1997). General difficulties in ABL determination within complex terrain (Staudt, 2006; Kalthoff et al., 1998; Kossmann et al., 1998) and the high background noise of the nearby street at BT01ETGS complicate the evaluation of the Sodar data. For most 'event days', no clear secondary maximum of reflectivity can be found for the daytime boundary layer evolution, thus making the determination of  $z_i$  a rough estimate rather than an exact determination.

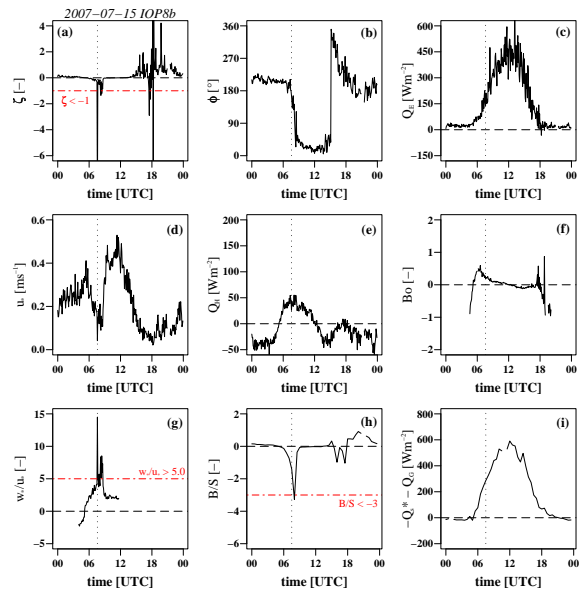


Figure 9: Stability parameter  $\zeta$  (a), wind direction (b),  $Q_E$  (c),  $u_*$  (d),  $Q_H$  (e),  $Bo$  (f),  $w_*/u_*$  (g),  $B/S$  (h) and available energy  $-Q_S - Q_G$  (i) for IOP8b at BT01ETGS. The black dotted lines in each graph indicate the time of the most vigorous event at 7:35 UTC.

However, Figure 8 shows the measured reflectivity of the Sodar/RASS complex, together with the determined evolution of  $z_i$  in the morning hours between 4:00 -11:40 UTC indicated as black

points, thus enabling the display of  $w/u$  in Figure 9g at the same time. Additionally, Figure 9h depicts the ratio  $B/S$ , where the wind shear – necessary for the calculation of  $S$  – was determined with the wind speeds measured with the cup anemometers at the profile mast in 4 and 9 m a.g.l. Considering the canopy height of 2.4 m at that time results in aerodynamic measurement heights  $z_a$  of 2.4 m and 7.4 m, respectively. The remarkable minima in Figure 9h at the times of the FCEs (7:35 till 8:40 UTC) shows that the turbulence is mainly driven by buoyancy rather than shear forces.

Up to this point, the surface-induced generation of FCEs at IOP8b has been described in detail; now its contribution to possible cloud formation or even precipitation events over the COPS area shall be discussed. Satellite imagery (not depicted) did not reveal the formation of clouds over the Kinzig valley on this day. Nevertheless, the formation of some isolated fair-weather cumuli at IOP8b, which can be associated with the FCEs, cannot be excluded but are not detectable using satellite imagery due to the sub-scale characteristics of these clouds.

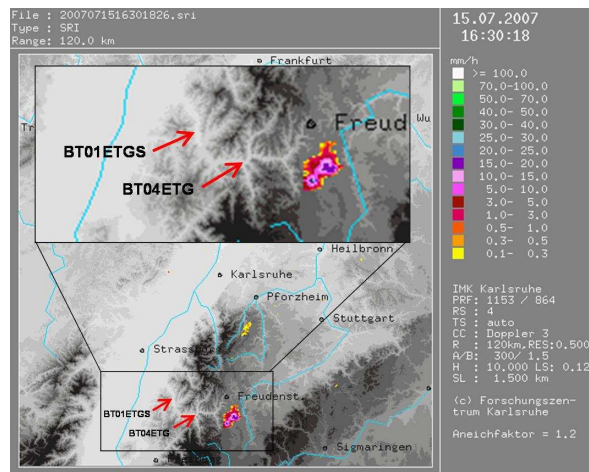


Figure 10: Radar image of the IMK Precipitation Radar (FZK) archive for IOP8b at 14:30 UTC obtained from <http://www.cops2007.de/>. The depicted rain rate [mm/h] reveals the formation of a single, precipitating cell at about 30 km south of Freudenstadt nearby the upper Kinzig valley. The locations of BT01ETGS and BT04ETG are indicated by red arrowheads. Both stations showed the occurrence of FCEs at IOP8b.

Moreover, a single deep convective cell, which formed at IOP8b in the vicinity of the upper Kinzig valley visible from radar data in Figure 10, might experience a FCE-related contribution to its pre-convective environment, as vertical dislocated

amounts of heat and moisture originating from the FCEs in the Kinzig valley might be transported with the up-valley and synoptical winds towards the spot of onset of the cell. This assumption is supported if the eastward directed valley structure is considered to be facilitating the large-scale flow dislocation due to channelling effects.

Now, having outlined the generation of FCEs due to a change of the valley wind system in detail for COPS IOP8b, the entire measurement period should be regarded. At BT01ETGS, 23 days, which make up 25 % of the 92 days observed in the COPS field campaign, can be classified as ‘event days’ coinciding with the above-outlined paradigm of COPS IOP8b. Furthermore, 19 days (21%) can be denoted as ‘intermittent days’, as they do not exhibit a clear diurnal, persistent valley wind circulation. FCEs occur but can only be attributed to brief duration –several minutes up to a few hours– changes from down-valley to up-valley winds during the day, these sometimes not even reaching a full wind rotation of 180°. Despite the fact that most of the FCEs of these ‘intermittent days’ seem to be triggered by short changes of wind direction of varying duration, it was decided to separate the ‘intermittent’ from the ‘event days’ in order to have similar flow patterns initiating the FCEs and thus a clear structured dataset. The reason for the intermittence of the valley winds is a decrease of the solar energy input, e.g. due to cloud shading, which possibly could be ascribed to the formerly initiated free convection events in the morning hours providing the needed heat and moisture for the initiation of clouds. Finally, 37 days (40%) at BT01ETGS can be characterized as ‘non-event days’, as FCEs are not accompanied with a valley wind rotation or usually do not actually appear. 13 days (14%) could not be evaluated due to data failure.

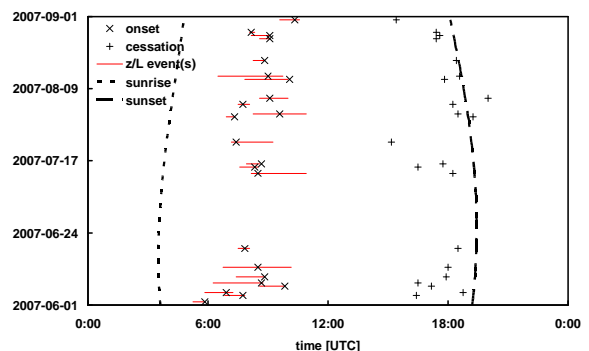


Figure 11: Onset and cessation times of the up-valley winds, free convection event times and the time of sunset and sunrise of the ‘event days’ at BT01ETGS.

Table 2: Mean onset and cessation times of the up-valley winds and the mean FCE times of those days classified as 'event days', with standard deviation, and number for the individual months and for the whole measurement period at BT01ETGS.

onset				cessation				z/L event(s)			
period	mean	stdev	number	period	mean	stdev	number	period	mean	stdev	number
june	8:01	1:14	8	june	17:36	0:55	7	june	7:33	1:08	8
july	8:03	0:37	5	july	17:23	1:35	5	july	8:14	0:51	5
august	9:06	0:46	10	august	17:56	1:10	10	august	8:48	0:42	10
whole	8:29	1:02	23	whole	17:42	1:10	22	whole	8:14	1:01	23

Figure 11 shows all days classified as 'event days' (23) with the onset and cessation times of the valley wind circulation system, the periods in which FCEs occurred and the times of sunrise and sunset valid for the COPS experiment period from June to August 2007. The mean onset and cessation times of the up-valley winds and the mean FCE times of those days classified as 'event days', with standard deviation and number are listed in Table 2 for the individual months and the whole measurement period. Remarkable is the adjustment of the onset of the up-valley winds and of the FCE times to the annual cycle of sunset evident in the mean values of the individual months. The mean duration of the periods in which FCEs occur – depicted in Figure 11 – is 1 h and 24 min with a standard deviation of 57 min.

To clarify the difference of 'event' and 'intermittent days' as related to the diurnal valley wind system, persistence values  $P$  were calculated from the EC sonic anemometer following Lugauer and Winkler (2005):

$$P(t) = \frac{\sqrt{\overline{u(t)^2} + \overline{v(t)^2}}}{\overline{v_h(t)}} \quad (4)$$

where the temporal vector mean of the horizontal wind speed is divided by the arithmetic mean of the horizontal wind speed at every time of the day.  $P$  can adopt values between 0 and 1, where 1 means that every day at that time the wind blew from the same direction. Figure 12 depicts the calculated persistence  $P$  for all days, 'event days', 'intermittent days' and 'non-event-days' at BT01ETGS. Two pronounced eye-catching minima can be found for the 'event days', i.e. one at the times the up-valley winds start (ca. 8:00 UTC) and another at the times the up-valley winds rotate back to down-valley winds (ca. 18:00 UTC), indicating highly variable wind directions during these times. The  $P$  values above 0.75 for the rest of the time point to a quasi identical flow pattern

for the 23 selected event days at BT01ETGS. The small persistence values of the intermittent days between 6 and 18 UTC can be attributed to the non-persistence of the up-valley winds, as briefly lasting up-valley winds are interrupted by frequent rotations back to the original wind direction due to a decrease of the solar energy input (through cloud shading) which otherwise usually drives the valley wind circulations.

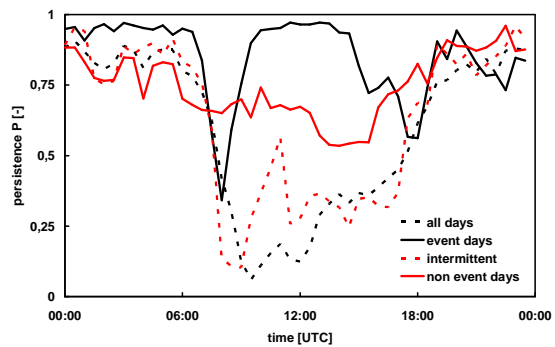


Figure 12: Persistence  $P$  for all days, with days classified as 'event days', 'intermittent days' and 'non-event-days' at BT01ETGS obtained from the EC sonic anemometer.

Mean diurnal courses of  $\zeta$  (Figure 13a),  $u$  (Figure 13b),  $Q_H$  (Figure 14a), global radiation (Figure 14b) and  $Q_E$  (Figure 14c) of the individually classified days can be applied to characterize the FCEs. Mean stability values  $\zeta$  indicate the occurrence of FCEs in the morning hours at about 8:00 UTC for both 'intermittent' and 'event days'. After this distinct minima of  $\zeta$  (until about 12:00 UTC), the 'intermittent days' show slightly lower  $\zeta$  values, indicating that the intermittence of the valley wind system causes more frequent triggering of FCEs. A clear gap in the magnitude of the  $u$ -values of the 'event' and 'non-event days' during the minimum of  $\zeta$  at about 8:00 UTC clarifies the capability of the morning hour valley

wind transition period to generate FCEs. During the evening transition period at about 18:00 UTC values of  $u_*$  of the 'event days' again fall below those of the 'non-event days'. The generally lower friction velocities for the 'intermittent days' can be explained by the non-persistence of the valley winds resulting in a continuous drop of the horizontal wind speed. Above-average values of  $Q_H$  and global radiation (Figure 14a and 14b) can be found for the event days, thus indicating the preferred initiation of FCEs in clear, undisturbed weather situations with high solar radiation driving the valley winds, which act as the trigger mechanism for the FCEs by providing a minimum of  $u_*$  in the early morning transition period. Moreover, about  $100 \text{ Wm}^{-2}$  higher  $Q_E$  values (Figure 14c) can be observed for the 'event days' compared to 'non-event days', which also contribute, due to density effects, to the destabilization of near-ground air masses and, if mixed into the ML, may support cloud formation. The formation of fair-weather cumuli on 'event days' at around midday due to surface-induced convective transport mechanisms may be deduced from the depicted global radiation (Figure 14b), as a drop from about 11:00 until 12:30 UTC deviates from the more or less bell-shaped course of the global radiation for the rest of the day.

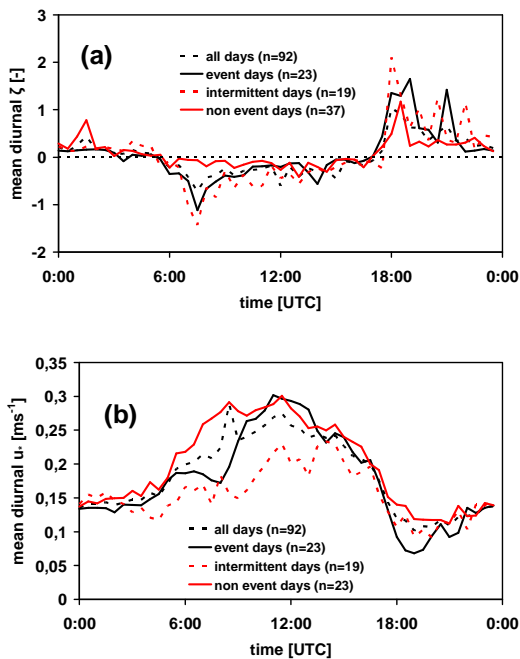


Figure 13: Mean diurnal courses of the stability parameter  $\zeta$  (a) and the friction velocity  $u_*$  (b) for all days of the measurement period (92), days classified as 'event days' (23), 'intermittent days' (19) and 'non-event days' (37) at BT01ETGS.

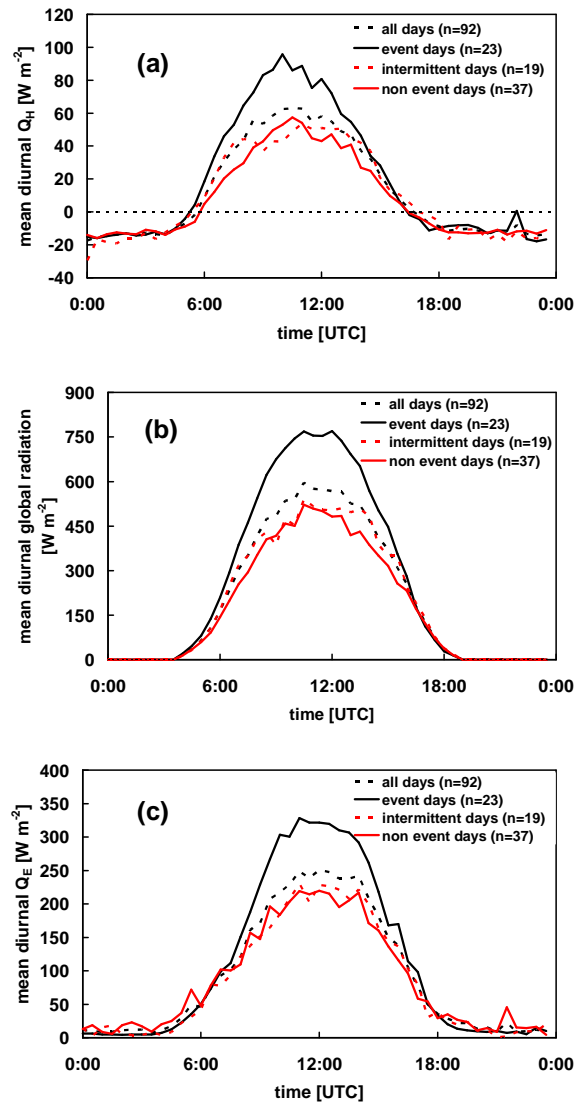


Figure 14: Mean diurnal courses of  $Q_H$  (a), global radiation (b) and  $Q_E$  (c) for all days of the measurement period (92), days classified as 'event days' (23), 'intermittent days' (19) and 'non-event days' (37) at BT01ETGS.

## 5. CONCLUSIONS

A comprehensive quality assurance and control effort, including footprint analysis and a check for internal boundary layers, was adapted to the energy exchange measurements of two energy balance stations incorporated in the COPS energy balance network in order to obtain high-quality surface flux data usable for further analysis. The energy exchange measurements led to the detection and description of free convection events (FCEs) in the morning hours, which were

found to be triggered by a change of the local circulation system. These FCEs occurred on about half of the total 92 days investigated during the COPS field campaign. This confirms the assumption of Mayer et al. (2008) that other regions –besides the alpine foreland investigated in their study– might face trigger mechanisms, such as local or meso-scale circulation systems leading to the convective release of near-ground air masses into the ABL. FCEs initiated by a change of the valley winds were also found by Hiller et al. (2008) in an alpine valley in Switzerland following their stability and data quality analysis. Unfortunately, these authors did not address these events. Eddy-covariance measurement systems and the thereby derived stability parameter  $\zeta$ , which indicates free convection situations for  $\zeta < -1$ , are able to detect such FCEs induced by local minima of the friction velocity  $u_*$  during the period of transition of the down-valley winds prevailing at night to up-valley winds in the early morning hours. Other parameters such as the ratio of the Deardorff velocity  $w_*$  to  $u_*$  and the ratio of B/S have been deduced in this study and confirm their capability to denote FCEs. To sum up, FCEs are likely to have –in addition to other orographic or landscape effects triggering convection– a not negligible impact on ABL temperature and moisture profiles. However, it must be noted that the measuring set-up with single turbulence point measurements cannot clarify the dimension and magnitude of the FCEs. The spatial extent of such plume-like FCEs is unclear, as it cannot be assumed that they are spatially limited to the target land use type for which the turbulent fluxes are being measured. Consequently, it is not possible to clarify the horizontal dimensions of the near-ground air masses destabilized and thus about the exact quantities of heat and moisture transported upwards into the ABL. Furthermore, the triggered turbulent pulse-like motions cannot be traced within the ABL, thus inhibiting detailed statements about the impact of these vertical transport mechanisms on local ABL thermodynamics and on possibly subsequent cloud formation. To address such questions, the application of large eddy simulation (LES) in order to directly simulate the behaviour of FCEs within the ABL would be desirable. This could be supported by using the energy exchange measurements of this study to supply initial field and boundary conditions for the model. Within the follow-on project SALVE, the application of LES will be utilized for further investigations.

## 6. ACKNOWLEDGEMENTS

The project was funded within the Priority Program 1167 'Quantitative Precipitation Forecast PQP (Praecipitationis Quantitativae Predictio)' by the German Science Foundation (DFG). The authors wish to acknowledge the support and data provision by the participants of the COPS experiment and the COPS Operations Center.

## 7. REFERENCES

- Aubinet, M., Grelle, A., Ibrom, A., Rannik, Ü., Moncrieff, J. B., Foken, T., Kowalski, A. S., Martin, P., Berbigier, P., Bernhofer, C., Clement, R., Elbers, J. A., Granier, A., Grünwald, T., Morgenstern, K., Pilegaard, K., Rebmann, C., Snijders, W., Valentini, R., Vesala, T., 2000. Estimates of the annual net carbon and water exchange of European forests: the EUROFLUX methodology. *Advances in Ecological Research*, 30: 113-175.
- Baldocchi, D., Falge, E., Gu, L. H., Olson, R., Hollinger, D., Running, S., Anthoni, P., Bernhofer, C., Davis, K., Evans, R., Fuentes, J., Goldstein, A., Katul, G., Law, B., Lee, X. H., Malhi, Y., Meyers, T., Munger, W., Oechel, W., Paw U, K. T., Pilegaard, K., Schmid, H. P., Valentini, R., Verma, S., Vesala, T., Wilson, K., Wofsy, S., 2001. FLUXNET: A new tool to study the temporal and spatial variability of ecosystem-scale carbon dioxide, water vapor, and energy flux densities. *Bulletin of the American Meteorological Society*, 82: 2415-2434.
- Beyrich, F., 1997. Mixing height estimation from SODAR data – a critical discussion. *Atmospheric Environment*, 31: 3941-3953.
- Deardorff, J.W., 1970a. Convective velocity and temperature scales for the unstable planetary boundary layer and for Rayleigh convection. *Journal of the Atmospheric Sciences*, 27: 1211–1213.
- Deardorff, J.W., 1970b. Preliminary results from numerical integration of the unstable planetary boundary layer. *Journal of the Atmospheric Sciences*, 27: 1209–1211.
- Eigenmann, R., 2008. Investigation of conditions initiating free convection using energy exchange measurements. COPS-experiment, Black Forest, 2007. Diploma thesis, University of Bayreuth, 127 pp.
- Foken, T., 2008a. *Micrometeorology*. Springer-Verlag, Heidelberg, 306 pp.

- Foken, T., 2008b. The energy balance closure problem - An overview. *Ecological Applications*, accepted.
- Foken, T., Göckede, M., Mauder, M., Mahrt, L., Amiro, B. D., und Munger, J. W., 2004. Post-field data quality control. In: X. Lee, W. Massman and B. Law (Editors), *Handbook of Micrometeorology: A Guide for Surface Flux Measurements*. Atmospheric and Oceanographic Sciences Library. Kluwer, Dordrecht, pp. 181-208.
- Foken, T., Wichura, B., 1996. Tools for quality assessment of surface-based flux measurements. *Agricultural and Forest Meteorology*, 78: 83-105.
- Foken, T., Wimmer, F., Mauder, M., Thomas, C., Liebethal, C., 2006. Some aspects of the energy balance closure problem. *Atmospheric Chemistry and Physics*, 6: 4395-4402.
- Göckede, M., Foken, T., Aubinet, M., Aurela, M., Banza, J., Bernhofer, C., Bonnefond, J.-M., Brunet, Y., Carrara, A., Clement, R., Dellwik, E., Elbers, J.A., Eugster, W., Fuhrer, J., Granier, A., Grünwald, T., Heinesch, B., Janssens, I.A., Knohl, A., Koeble, R., Laurila, T., Longdoz, B., Manca, G., Marek, M., Markkanen, T., Mateus, J., Matteucci, G., Mauder, M., Migliavacca, M., Minerbi, S., Moncrieff, J.B., Montagnani, L., Moors, E., Ourcival, J.-M., Papale, D., Pereira, J., Pilegaard, K., Pita, G., Rambal, S., Rebmann, C., Rodrigues, A., Rotenberg, E., Sanz, M.J., Sedlak, P., Seufert, G., Siebicke, L., Soussana, J.F., Valentini, R., Vesala, T., Verbeeck, H., Yakir, D., 2008. Quality control of CarboEurope flux data – Part 1: Coupling footprint analyses with flux data quality assessment to evaluate sites in forest ecosystems. *Biogeosciences*, 5: 433-450.
- Göckede, M., Markkanen, T., Hasager, C. B., und Foken, T., 2006. Update of a footprint-based approach for the characterisation of complex measurement sites. *Boundary-Layer Meteorology*, 118: 635-655.
- Göckede, M., Rebmann, C., und Foken, T., 2004. A combination of quality assessment tools for eddy covariance measurements with footprint modeling for the characterisation of complex sites. *Agricultural and Forest Meteorology*, 127: 175-188.
- Hiller, R., Zeeman, M.J., Eugster, W., 2008. Eddy-Covariance Flux Measurements in the Complex Terrain of an Alpine Valley in Switzerland. *Boundary-Layer Meteorology*, 127: 449-467.
- Inagaki, A., Letzel, M. O., Raasch, S., Kanda, M., 2006. Impact of surface heterogeneity on energy imbalance: A study using LES. *Journal of the Meteorological Society of Japan*, 84: 187-198.
- Jegede, O. O., Foken, T., 1999. A study of the internal boundary layer due to a roughness change in neutral conditions observed during the LINEX field campaigns. *Theoretical and Applied Climatology*, 62: 31-41.
- Kalthoff, N., Binder, H.J., Kossmann, M., Vögtlin, R., Corsmeier, U., Fiedler, F., Schlager, H., 1998. Temporal evolution and spatial variation of the boundary layer over complex terrain. *Atmospheric Environment*, 32: 1179-1194.
- Kanda, M., Inagaki, A., Letzel, M. O., Raasch, S., Watanabe, T., 2004. LES study of the energy imbalance problem with eddy covariance fluxes. *Boundary-Layer Meteorology* 110: 381-404.
- Kossmann, M., Vögtlin, R., Corsmeier, U., Vogel, B., Fiedler, F., Binder, H.J., Kalthoff, N., Beyrich, F., 1998. Aspects of the convective boundary layer structure over complex terrain. *Atmospheric Environment*, 32: 1323-1348.
- Liebethal, C., Foken, T., 2007. Evaluation of six parameterization approaches for the ground heat flux. *Theoretical and Applied Climatology*, 88: 43-56.
- Lugauer, M., Winkler, P., 2005. Thermal circulation in South Bavaria – climatology and synoptic aspects. *Meteorologische Zeitschrift*, 14: 15-30.
- Mauder, M. and T. Foken, 2004: Documentation and instruction manual of the eddy covariance software package TK2. Work Report University of Bayreuth, Department of Micrometeorology, 26, 44 pp., ISSN 1614-8916.
- Mauder, M., Liebethal, C., Göckede, M., Leps, J.P., Beyrich, F., Foken, T., 2006. Processing and quality control of flux data during LITFASS-2003. *Boundary-Layer Meteorology*, 121: 67-88.
- Mayer, J.C., Staudt, K., Gilge, S., Meixner, F.X., Foken, T., 2008. The impact of free convection on late morning ozone decreases on an Alpine foreland mountain summit. *Atmospheric Chemistry and Physics, Discussion*, 8: 5437–5476.
- Meißner, C., Kalthoff, N., Kunz, M., Adrian, G., 2007. Initiation of shallow convection in the Black Forest mountains. *Atmospheric Research*, 86: 42-60.
- Metzger, S., Foken, T., Eigenmann, R., Kurtz, W., Serafimovich, A., Siebicke, L., Olesch, J., Staudt, K., Lüers, J., 2007. COPS experiment, Convective and orographically induced precipitation study, 01 June 2007 – 31 August

- 2007, Documentation. Work Report University of Bayreuth, Department of Micrometeorology, 34, 72 pp., ISSN 1614-8916.
- Raabe, A., 1983. On the relation between the drag coefficient and fetch above the sea in the case of off-shore wind in the near shore zone. *Zeitschrift für Meteorologie*, 33: 363-367.
- Rannik, Ü., Markkanen, T., Raittala, J., Hari, P., und Vesala, T., 2003. Turbulence statistics inside and over forest: Influence on footprint prediction. *Boundary-Layer Meteorology*, 109: 163-189.
- Rannik, Ü., Aubinet, M., Kurbanmuradov, O., Sabelfeld, K. K., Markkanen, T., Vesala, T., 2000. Footprint analysis for measurements over a heterogeneous forest. *Boundary-Layer Meteorology*, 97: 137-166.
- Rebmann, C., Göckede, M., Foken, T., Aubinet, M., Aurela, M., Berbigier, P., Bernhofer, C., Buchmann, N., Carrara, A., Cescatti, A., Ceulemans, R., Clement, R., Elbers, J. A., Granier, A., Grunwald, T., Guyon, D., Havrankova, K., Heinesch, B., Knohl, A., Laurila, T., Longdoz, B., Marcolla, B., Markkanen, T., Miglietta, F., Moncrieff, J., Montagnani, L., Moors, E., Nardino, M., Ourcival, J. M., Rambal, S., Rannik, U., Rotenberg, E., Sedlak, P., Unterhuber, G., Vesala, T., und Yakir, D., 2005. Quality analysis applied on eddy covariance measurements at complex forest sites using footprint modelling. *Theoretical and Applied Climatology*, 80: 121-141.
- Savelyev, S. A., Taylor, P. A., 2005. Internal boundary layers: I. Height formulae for neutral and diabatic flows. *Boundary-Layer Meteorology*, 115: 1-25.
- Staudt, K., 2006. Determination of the atmospheric boundary layer height in complex terrain during SALSA 2005. Diploma thesis, University of Bayreuth, 112 pp.
- Steinfeld, G., Letzel, M. O., Raasch, S., Kanda, M., Inagaki, A., 2007. Spatial representativeness of single tower measurements and the imbalance problem with eddy-covariance fluxes: results of a large-eddy simulation study. *Boundary-Layer Meteorology*, 123: 77-98.
- Whiteman, C.D., 1990. Observations of thermally developed wind systems in mountainous terrain. In: W. Blumen (Editor), *Atmospheric Processes over Complex Terrain*. *Meteorological Monographs*, 23 (45), American Meteorological Society, Boston, USA, Chapter 2, pp. 5-42.
- Winkler, P., Lugauer, M., Reitebuch, O., 2006. *Alpines Pumpen*. *promet*, 32: 34-42.
- Wulfmeyer, V., Behrendt, A., Adrian, G., Althausen, D., Aoshima, F., Baelen, J.v., Barthlott, C., Bauer, H.-S., Blyth, A., Brandau, C., Corsmeier, U., Craig, G., Crewell, S., Dick, G., Dorninger, M., Dufournet, Y., Ehret, G., Engelmann, R., Flamant, C., Foken, T., Hauck, C., Girolamo, P.D., Graßl, H., Grzeschik, M., Handwerker, J., Hagen, M., Hardesty, R.M., Hauck, C., Junkermann, W., Kalthoff, N., Kiemle, C., Kottmeier, C., Krauss, L., Long, C., Lelieveld, J., Madonna, F., Miller, M., Mobbs, S., Neininger, B., Pal, S., Peters, G., Radlach, M., Richard, E., Rotach, M., Russchenberg, H., Schlüssel, P., Schumann, U., Simmer, C., Steinacker, R., Turner, D., Vogt, S., Volkert, H., Weckwerth, T., Wernli, H., Wieser, A., Wunrau, C., 2007. Convective and Orographically-induced Precipitation Study. COPS Field Report 2.1., <https://www.uni-hohenheim.de/spp-iop/documents/COPSPFieldReport2.pdf>.